A Feature-based Approach on Contact-less Blood Pressure Estimation from Video Data

Carolin Wuerich
Fraunhofer IMS
Duisburg, Germany
carolin.wuerich@ims.fraunhofer.de

Eva-Maria Humm
Fraunhofer IMS
Duisburg, Germany
eva.humm97@web.de

Christian Wiede
Fraunhofer IMS
Duisburg, Germany
christian.wiede@ims.fraunhofer.de

Gregor Schiele
Embedded Systems,
University of Duisburg-Essen
Duisburg, Germany
gregor.schiele@uni-due.de

***Abstract*—Conventional blood pressure monitors and sensors have several limitations in terms of accuracy, measurement time, comfort or safety. To address these limitations, we realized and tested a surrogate-based contact-less blood pressure estimation method which relies on a single remote photoplethysmogram (rPPG) captured by camera. From this rPPG signal, we compute 120 features, and perform a sequential forward feature selection to obtain the best subset of features. With a multilayer perceptron model, we obtain a mean absolute error ± standard deviation of MAE 5.50 ±4.52 mmHg for systolic pressure and 3.73 ±2.86 mmHg for diastolic pressure. In contrast to previous studies, our model is trained and tested on a data set including normotensive, pre-hypertensive and hypertensive values.**

***Index Terms*—blood pressure, remote photoplethysmography, feature selection, neural network**

I. Introduction

Blood pressure is an important vital parameter and deviations from the normal range can cause serious health issues or indicate changes in a patients health status. It is commonly measured with a sphygmomanometer or in very critical situations invasively with a catheter. However, cuff-based devices allow only discrete measurements and are uncomfortable for the patient. Invasive measurements on the other hand involve a risk of infection and thrombosis and are therefore not used for general blood pressure monitoring. To overcome these limitations, recent studies investigated beat-to-beat blood pressure estimation from surrogate parameters [1]–[3] such as photoplethysmogram (PPG) and electrocardiogram (ECG). Such approaches can be transferred to completely contact-less blood pressure estimation methods. Contact-less methods enable more hygienic, comfortable and beat-to-beat measurements and could be employed not only in the hospital and health care settings, but also as smartphone applications encouraging more regular ambulatory measurements. In this paper, we present an approach on blood pressure estimation via camera which employs PPG signal feature extraction and selection, and finally a multilayer perceptron (MLP) regression. In contrast to previous studies on camera-based blood pressure measurement, our training and test data set includes normotensive, pre-hypertensive and hypertensive pressure values and a feature selection is performed to increase overall relevance of the input data.

II. Related Work

In the last decade, new approaches on cuff-less surrogate-based blood pressure measurement receive increased attention. Most published methods are based on pulse wave velocity (PWV) which can be obtained by measuring the temporal delay of a pulse wave between two specified locations. One possibility to measure this delay is the pulse arrival time (PAT) calculated as the time difference from the r-peak of the electrocardiogram (ECG), i.e. the contraction of the heart, and the rising edge of the photoplethysmogram (PPG) [4], [5]. Another common method is based on two PPG signals at different distances from the heart to obtain the differential pulse transit time (dPTT) [6]–[9]. Zhang et al. [5] compared these two parameters against invasively measured blood pressure. In their study, the regression based on PAT obtained an RMSE value over twice as large as the one based on dPTT and did not meet FDA blood pressure limits. They explain this difference by the varying pre-ejection period which is contained in the PAT but not in the PTT. However, also PTT-based predictions have limitations. Jeong and Finkelstein [9] observed a different slope of the regression curve for each subject such that individual calibrations are required. Further, the relative positional relationship of the two measurement locations needs to be maintained.

Therefore, more recent approaches consider signal morphology of the PPG in addition to the PAT value [2], [10], [11] or PPG morphology only [1], [12]–[14]. Whereas former methods require ECG and thus body-worn devices, latter ones can be applied on contact-less PPG signals. Few papers have been published on these feature-based models for remote or camera-based PPG (rPPG) [3], [15], [16]. Jain and Subramanyam [15] extract their rPPG from the red RGB channel by stacking the channel information of all frames and applying a principal component analysis (PCA) to remove noise. Next, they extract features from the best part of the signal. This includes mostly time domain features and the dominant frequency. With a polynomial kernel regression they obtain a MAE of 3.9 ±5.4 mmHg for systolic pressure (SBP) and 3.7 ±5.1 mmHg for diastolic pressure (DBP) on normotensive subjects with DBP between 60 and 90 mmHg and SBP between 95 and 130 mmHg only. Lou at al. [3] use a smart phone camera for the signal acquisition and transform the 8-bit encoded images into

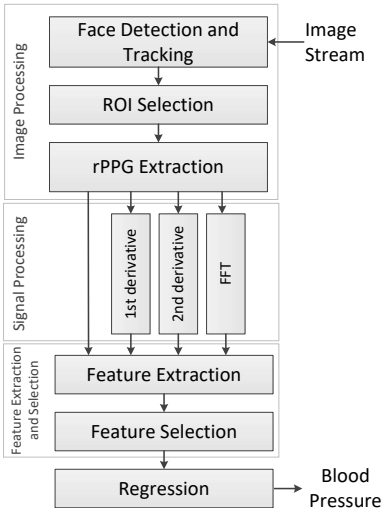

Fig. 1. Pipeline for camera-based blood pressure estimation.

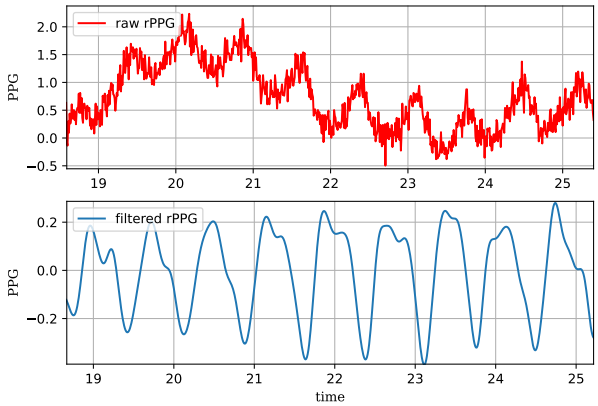

Fig. 2. The upper plot depicts the raw rPPG signal and the lower one shows the filtered and inverted signal which is used for further processing.

8 separate bit layers. For rPPG extraction, they isolate those layers where the bits fluctuate along with continuous reference blood pressure. From data of 1328 subjects, 155 signal features were extracted including pulse amplitude, shape and frequency features. Lou at al. [3] employ PCA for dimensionality reduction producing 30 eigenvectors which are used as input for a multi-layer perceptron model. They obtained a ME of 0.4 $\pm$7.3 mmHg for SBP and -0.2 $\pm$6.0 mmHg for DBP. However, their subjects were specifically selected with DBP only between 60 and 89 mmHg and SBP between 100 and 139 mmHg, too. Further, a dimensionality reduction compresses all information into fewer features, but does not differentiate between relevant and irrelevant information. In contrast, we employ a feature selection method to only include those features that contribute most to blood pressure prediction.

III. Proposed Method

Figure 1 illustrates the pipeline of the proposed method. The approach starts with an image processing part to extract the remote PPG from videos. For this, face detection is performed and skin pixels are extracted from the forehead. This is followed by a signal processing part in which the PPG signal is filtered and derivatives as well as the frequency spectrum are computed. For the PPG signal and these representations of it, 120 different signal features are defined as input candidates for the regression model. To obtain a subset of relevant features for the prediction problem, sequential feature selection is performed. Finally, we train a neural network for blood pressure prediction.

A. Image Processing

The PPG signal is extracted from facial skin pixels. For the detection of the face, we employ a Single Shot Detector (SSD) [17]. Based on the resulting bounding box, the position and size of the ROI is determined such that it is placed over the forehead. After face detection in the first frame, tracking of the corresponding area is performed in subsequent images to reduce movement artefacts and processing time. The filter-based Minimum Output Sum of Squared Error (MOSSE) method [18] showed to be the most stable tracker for this task with a stability of 99.9 % and no tracking failure in our experimental setup. Hence, signal distortions from faulty face tracking did not influence our results. Finally, the PPG signal is extracted from the green channel of the ROI, since for haemoglobin, the absorption of the light peaks in the green spectrum. Cui et al. [19] observed a prominent maximum in the reflectance pulsation spectrum around 575 nm during their studies of in vivo reflectance of blood and skin tissue at various wavelengths. Therefore, the signal is obtained as the mean pixel intensity $\bar{I}_G(t)$ of the green channel G of all n pixels within the ROI over time t:

$$\bar{I}_G(t) = \frac{1}{n} \sum_{x \in ROI} I_{G,x}(t) \tag{1}$$

B. Signal Processing

The obtained raw rPPG signal contains a lot of noise and the blood volume pulses are modulated by the respiratory signal as shown in Figure 2. To reduce noise and level the signal, we apply two low-pass FIR filters. The first one has a cut-off frequency of 0.3 Hz, such that the respiration signal up to 20 breaths per minute remains. This signal is subtracted from the original signal and finally, the second filter with a cut-off frequency of 6 Hz removes high-frequency noise while preserving the PPG waveform.

C. Feature Extraction and Selection

We defined 120 features to describe the PPG signal. Time domain features are extracted for each PPG cycle whereas frequency domain features are computed for a signal segment of 5 seconds. The cycle detection is based on the maxima positions of the first derivative which represent the steepest point of the systolic up-slopes [13]. A sliding window which spans one and a half average cycles ensures that only the largest maximum values in the neighborhoods are kept and hence, diastolic peaks or potential double peaks are not chosen. For

TABLE I
FEATURE TYPES EXTRACTED FROM PPG SIGNAL

Feature type	Description
Pulse width	Pulse width for systolic, diastolic and whole cycle, and ratios. Also, pulse width (systolic, diastolic and ratios) at various heights between minimum and systolic peak.
Amplitudes	Amplitudes of the PPG signal and of its first and second derivative, as well as ratios of the amplitudes.
Area under curve	Integral for systolic, diastolic and whole cycle, and ratios of them.
FFT amplitudes	Amplitudes in the signal's frequency spectrum up to 4.6 Hz.
Max. power frequencies	Frequencies with the highest spectral densities in descending order.
External features	Sex, height, weight, and age of the subject.

this, the average cycle length is obtained from the dominant frequency in the Fourier-transformed signal segment. Finally, the minimum before the chosen systolic up-slope is defined as the beginning of a cycle and the maximum afterwards is the systolic peak. The dicrotic notch is identified as last minimum before the end of the cycle or, if no minimum is found for inflection type dicrotic notches, as last maximum in the first derivative, respectively. Only cycles with a dicrotic notch detected and a length within 0.67 - 1.67 times the average cycle length are considered for further processing in order to remove corrupted pulses. The values are chosen empirically.
Table I gives an overview of extracted signal features. Time domain features include width, amplitude and area under the curve for systolic and diastolic cycles as well as ratios between these values. Another group of features contains systolic and diastolic widths at different heights of the pulse. From the first and second derivative, we extracted amplitudes for the first three extrema. Frequency domain features include the maximum power frequencies and their amplitudes.
Since not all of these 120 features contain relevant information for blood pressure prediction, a sequential forward feature selection is performed. Only those features that can contribute to prediction accuracy are selected as input for the regression model. The numbers of chosen features lie between 15 and 20.

D. Regression Model

A Random Forest Regression (RFR) model and an MLP are trained as single-output regressions for systolic and diastolic blood pressure separately and as two-output architectures. Hyper-parameter tuning is performed for the MLP to obtain the best model. The best model is selected based on a 10-fold cross-validation and finally tested on an independent test set. For the DBP single-output MLP, we obtained a model of 16 inputs and two hidden layers with 500 and 50 neurons, and for SBP, a model with 17 inputs and two hidden layers of 100 and 1000 neurons performed best. As optimizer, we chose stochastic gradient descent (SGD) and all layers have ReLU activations.

IV. EXPERIMENTS

For training and validation of the method, we recorded a total of 150 videos of five subjects. Each video has a duration of 30 s at a sampling rate of 120 frames per second and 352 x 198 pixels. An Allied Vision Manta G-201-30fps camera was used with an exposure time of 5 ms. For the videos, subjects were seated in front of a plain wall and held their right hands next to their faces. The only light source was a window facade providing natural illumination. Before and after every recording, reference blood pressure was measured using a sphygmomanometer boso medicus X by BOSCH+SOHN GmbH. The sphygmomanometer was clinically validated according to protocol by the European Society of Hypertension (ESH) and exhibits a standard deviation (SD) of ± 3 mmHg. All subjects (two male, three female) were healthy and normotensive, aged between 24 and 27 years and weight between 54 to 85 kg. To obtain a wider range of blood pressure values, subjects had to do physical exercise (1 min plank or squats) before five of the measurements, and concentrate on deep and slow breathing before the next five measurements. Mori et al. [20] showed, that these breathing exercises lower blood pressure immediately by an average of 6.4 mmHg for normotensives and 9.6 mmHg for hypertensives. Finally, our dataset includes DBP values from 65 to 110 mmHg and SBP values from 95 to 180 mmHg. The recorded videos are separated into 5-second sections with 1 second overlap and blood pressure reference values are interpolated accordingly. With all PPG cycles deleted which do not meet the previously described criteria, we obtained an overall of 1088 data points.

V. RESULTS AND DISCUSSION

A. Results

In the sequential forward feature selection for DBP prediction, the first features being selected are amplitudes of the Fourier-transformed signal. Mainly, frequencies between 3.6 to 4.2 Hz are included, and later, frequencies between 0.8 to 1.4 Hz. The lower frequency range might represent the heart rate and the overall PPG pulse shape while the higher frequency range comprises details about dicrotic notch and systolic peak morphology. These frequency features also show a comparatively strong correlation with both DBP and SBP which coincides with [3]. As a fourth feature, an amplitude ratio of the PPG's second derivative, i.e. acceleration of the PPG signal, is added. Furthermore, the eighth to tenth most dominant frequencies of the signal are considered valuable for diastolic pressure prediction and finally, area and time features of the original PPG signal are chosen, but hereof mostly features representing ratios between the systolic and diastolic cycle or between diastolic area and time. In comparison, systolic pressure prediction does not seem to benefit much from derivative information. Instead, it mainly relies on amplitudes in the frequency domain between 3.4 to 4.2 Hz and lower frequencies from 1.2 to 1.6 Hz. In addition to the eighth to tenth most dominant frequency, also the first and second most dominant ones appear in the selection results. These frequency peaks usually lie around 6 Hz and exhibit a strong correlation with SBP, but not with DBP.

On the test set, the single-output MLP model for DBP obtained a mean absolute error (MAE $\pm$SD) of 4.04 $\pm$3.79

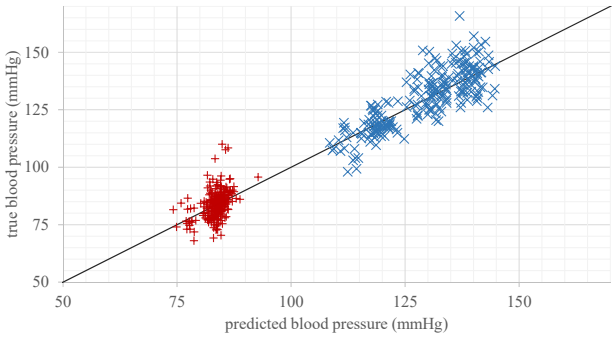

Fig. 3. Test data predictions of separate MLP regressions plotted against ground truth. Diastolic blood pressure is represented by +, and systolic pressure by x.

mmHg and an RMSE of 5.54 mmHg. The Pearson correlation coefficient for diastolic pressure prediction is $r = 0.44$.
For single-output MLP SBP prediction, test results show an MAE of 5.50 ±4.52 mmHg and an RMSE of 7.12 mmHg. The Pearson correlation coefficient is $r = 0.82$. The MAE on test data in the normotensive range (DBP from 60 to 90 mmHg and SBP from 95 to 140 mmHg) is 3.32 ±2.63 mmHg and 4.62 ±3.52 mmHg for diastolic and systolic pressure, respectively. Figure 3 depicts the predictions of these models and corresponding ground truth values for the test data. The two-output MLP performs worse for SBP but DBP seems to benefit from the additional backpropagated output information. This model obtains an MAE of 3.73 ±2.86 mmHg and 7.44 ±5.28 mmHg for diastolic and systolic pressure, respectively. However, the Pearson correlation coefficient for DBP predictions remains low with $r = 0.47$. The RFR models obtain higher prediction errors than the MLPs, for single-output as well as for the joint model as detailed in Table II.

B. Discussion

With the overall best results of an MAE of 5.50 ±4.52 mmHg for SBP and 3.73 ±2.86 mmHg for DBP on the whole test set, our method is within the standard set by the US Association for the Advancement of Medical Instrumentation (AAMI) of a maximum mean error < 5 mmHg and standard deviation < 8 mmHg [21] and obtains grade A for DBP and B for SBP (see Table II) according to Criteria of British Society of Hypertension (BSH) [22]. These are the two most widely used protocols which are also employed by the ESH.
The experiments show that MLP performs better for the given task than RFR, however, for both methods, DBP prediction benefits from including SBP in the learning process of the two-output models. Due to the larger range of SBP values, inclusion of those might encourage a wider spreading of DBP prediction values. Accordingly, the joint models limit the performance of SBP prediction because of the smaller range of DBP values.
In lack of publicly available data sets for the topic of contactless blood pressure estimation, we created our own data set. It still contains few subjects, all young, Caucasian and healthy.

TABLE II
BLOOD PRESSURE ESTIMATION RESULTS (IN MMHG)

Separate MLP (single-output)		
	Systolic Pressure	**Diastolic Pressure**
MAE±SD[a]	5.50±4.52	4.04±3.79
ME±SD	-0.85±7.07	0.04±5.54
RMSE[b]	7.12	5.54
Pearson coeff.	0.82	0.44
BSH[c] Grade	B	A
Joint MLP (two-output)		
	Systolic Pressure	**Diastolic Pressure**
MAE±SD[a]	7.44±5.28	3.73±2.86
ME±SD	-0.55±9.11	-0.27±4.70
RMSE[b]	9.12	4.71
Pearson coeff.	0.66	0.47
BSH[c] Grade	B	A
Separate RFR (single-output)		
	Systolic Pressure	**Diastolic Pressure**
MAE±SD[a]	6.00±5.62	4.68±3.99
ME±SD	0.35±8.22	-0.79±6.15
RMSE[b]	8.22	6.16
Pearson coeff.	0.77	0.26
BSH[c] Grade	B	A
Joint RFR (two-output)		
	Systolic Pressure	**Diastolic Pressure**
MAE±SD[a]	7.68±6.16	4.36±3.42
ME±SD	0.79±9.81	0.32±5.53
RMSE[b]	9.84	5.53
Pearson coeff.	0.69	0.37
BSH[c] Grade	B	A

[a]mean absolute error ± standard deviation, [b]root mean square error, [c]British Society of Hypertension

More - and more diverse - data will be collected in the future for improving the model and testing generalization capabilities for unseen subjects. It is worth highlighting that due to physical exercises, we obtained a larger range of blood pressure values than other studies did [3], [15]. In the future, it is desirable to have a public benchmark data set to enable comparability of published methods. When removing test data with blood pressure values outside the normotensive range, test results improve significantly to 3.32 ±2.63 mmHg (DBP) and 4.62 ±3.52 mmHg (SBP). This indicates a reduced fit of the model for hypertensive values, which may be caused by an underrepresentation of high pressure values in the data set or by differing correlations of the higher pressure range with the selected features. For normotensive DBP, we obtain better prediction results than previous studies [3], [15]. However, the corresponding Pearson coefficient still only reaches a value of $r = 0.47$ raising the question about the possibility of DBP prediction from rPPG waveforms with the amount of detail captured by camera. More research is needed to evaluate prediction capabilities. Further, the natural light in the study room appeared to be a disadvantage for the employed rPPG extraction method. When only considering the green channel for rPPG extraction, its values not only depend on color, but they are also very sensitive to illumination changes. Transforming the images into color spaces where illumination is

separated from color information might prevent such artefacts. Another limitation of our data set are the reference values. A linear interpolation might not represent the true development of blood pressure, especially for videos after physical exercise where blood pressure slowly normalizes within the 30 seconds of recording time. Also, it has to be noted that the reference device exhibits a measurement standard deviation of ± 3 mmHg.

VI. Summary and Future Work

We presented a camera-based method for contact-less blood pressure estimation, and trained and tested the model on a data set including normotensive, pre-hypertensive and hypertensive pressure values. The obtained MAE of 5.50 $\pm$4.52 mmHg for SBP and 3.73 $\pm$2.86 mmHg for DBP are within the AAMI standard and obtain grade B and A, respectively. In the future, we are going to further optimize rPPG extraction from video by transforming the images into another color space where color information can be separated from illumination values. Also, the method needs to be validated on a larger and more divers data set.

References

[1] Xing, Xiaoman ; Sun, Mingshan: Optical blood pressure estimation with photoplethysmography and FFT-based neural networks. In: *Biomedical optics express* 7 (2016), Nr. 8, S. 3007–3020. http://dx.doi.org/10.1364/BOE.7.003007. – DOI 10.1364/BOE.7.003007. – ISSN 2156–7085

[2] Yan, Cong ; Li, Zhenqi ; Zhao, Wei ; Hu, Jing ; Jia, Dongya ; Wang, Hongmei ; You, Tianyuan: Novel Deep Convolutional Neural Network for Cuff-less Blood Pressure Measurement Using ECG and PPG Signals. In: *Annual International Conference of the IEEE Engineering in Medicine and Biology Society. IE* 2019 (2019), S. 1917–1920. http://dx.doi.org/10.1109/EMBC.2019.8857108. – DOI 10.1109/EMBC.2019.8857108

[3] Luo, Hong ; Yang, Deye ; Barszczyk, Andrew ; Vempala, Naresh ; Wei, Jing ; Wu, Si J. ; Zheng, Paul P. ; Fu, Genyue ; Lee, Kang ; Feng, Zhong-Ping: Smartphone-Based Blood Pressure Measurement Using Transdermal Optical Imaging Technology. In: *Circulation. Cardiovascular imaging* 12 (2019), Nr. 8, S. e008857. http://dx.doi.org/10.1161/CIRCIMAGING.119.008857. – DOI 10.1161/CIRCIMAGING.119.008857

[4] Ghosh, Shrimanti ; Banerjee, Ankur ; Ray, Nilanjan ; Wood, Peter W. ; Boulanger, Pierre ; Padwal, Raj: Continuous blood pressure prediction from pulse transit time using ECG and PPG signals. In: *2016 IEEE Healthcare Innovation Point-Of-Care Technologies Conference (HI-POCT)*, IEEE, 112016. – ISBN 978–1–5090–1166–7, S. 188–191

[5] Zhang, Guanqun ; Gao, Mingwu ; Da Xu ; Olivier, N. B. ; Mukkamala, Ramakrishna: Pulse arrival time is not an adequate surrogate for pulse transit time as a marker of blood pressure. In: *Journal of applied physiology (Bethesda, Md. : 1985)* 111 (2011), Nr. 6, S. 1681–1686. http://dx.doi.org/10.1152/japplphysiol.00980.2011. – DOI 10.1152/japplphysiol.00980.2011

[6] Fan, Xijian ; Ye, Qiaolin ; Yang, Xubing ; Choudhury, Sruti D.: Robust blood pressure estimation using an RGB camera. In: *Journal of Ambient Intelligence and Humanized Computing* 11 (2020), Nr. 11, S. 4329–4336. http://dx.doi.org/10.1007/s12652-018-1026-6. – DOI 10.1007/s12652–018–1026–6. – ISSN 1868–5137

[7] Nakano, Kazuya ; Ohnishi, Takashi ; Nishidate, Izumi ; Haneishi, Hideaki: Noncontact sphygmomanometer based on pulse-wave transit time between the face and hand. In: Coté, Gerard L. (Hrsg.): *Optical Diagnostics and Sensing XVIII: Toward Point-of-Care Diagnostics*, SPIE, 27.01.2018 - 01.02.2018. – ISBN 9781510614871, 34

[8] Huang, Po-Wei ; Lin, Chun-Hao ; Chung, Meng-Liang ; Lin, Tzu-Min ; Wu, Bing-Fei: Image based contactless blood pressure assessment using Pulse Transit Time. In: *2017 International Automatic Control Conference (CACS)*, IEEE, 112017. – ISBN 978–1–5386–3900–9, S. 1–6

[9] Jeong, In C. ; Finkelstein, Joseph: Introducing Contactless Blood Pressure Assessment Using a High Speed Video Camera. In: *Journal of medical systems* 40 (2016), Nr. 4, S. 77. http://dx.doi.org/10.1007/s10916-016-0439-z. – DOI 10.1007/s10916–016–0439–z

[10] Kachuee, Mohammad ; Kiani, Mohammad M. ; Mohammadzade, Hoda ; Shabany, Mahdi: Cuffless Blood Pressure Estimation Algorithms for Continuous Health-Care Monitoring. In: *IEEE transactions on bio-medical engineering* 64 (2017), Nr. 4, S. 859–869. http://dx.doi.org/10.1109/TBME.2016.2580904. – DOI 10.1109/TBME.2016.2580904

[11] Paviglianiti, Annunziata ; Randazzo, Vincenzo ; Pasero, Eros ; Vallan, Alberto: Noninvasive Arterial Blood Pressure Estimation using ABPNet and VITAL-ECG. In: *2020 IEEE International Instrumentation and Measurement Technology Conference (I2MTC)*, IEEE, 52020. – ISBN 978–1–7281–4460–3, S. 1–5

[12] Fujita, Daisuke ; Suzuki, Arata ; Ryu, Kazuteru: PPG-Based Systolic Blood Pressure Estimation Method Using PLS and Level-Crossing Feature. In: *Applied Sciences* 9 (2019), Nr. 2, S. 304. http://dx.doi.org/10.3390/app9020304. – DOI 10.3390/app9020304

[13] Slapnikar, Gasper ; Lustrek, Mitja: Continuous Blood Pressure Estimation from PPG Signal.

[14] Li, Peihao ; Laleg-Kirati, Taous-Meriem: Central Blood Pressure Estimation from Distal PPG Measurement using semiclassical signal analysis features. In: *IEEE Access* 9 (2021), S. 44963–44973

[15] Jain, Monika ; Deb, Sujay ; Subramanyam, A V.: Face video based touchless blood pressure and heart rate estimation. In: *2016 IEEE 18th International Workshop on Multimedia Signal Processing (MMSP)* IEEE, 2016, S. 1–5

[16] Sugita, Norihiro ; Yoshizawa, Makoto ; Abe, Makoto ; Tanaka, Akira ; Homma, Noriyasu ; Yambe, Tomoyuki: Contactless Technique for Measuring Blood-Pressure Variability from One Region in Video Plethysmography. In: *Journal of Medical and Biological Engineering* 39 (2019), Nr. 1, S. 76–85. http://dx.doi.org/10.1007/s40846-018-0388-8. – DOI 10.1007/s40846–018–0388–8. – ISSN 1609–0985

[17] Liu, Wei ; Anguelov, Dragomir ; Erhan, Dumitru ; Szegedy, Christian ; Reed, Scott ; Fu, Cheng-Yang ; Berg, Alexander C.: Ssd: Single shot multibox detector. In: *European conference on computer vision* Springer, 2016, S. 21–37

[18] Bolme, David S. ; Beveridge, J R. ; Draper, Bruce A. ; Lui, Yui M.: Visual object tracking using adaptive correlation filters. In: *2010 IEEE computer society conference on computer vision and pattern recognition* IEEE, 2010, S. 2544–2550

[19] Cui, Weijia ; Ostrander, Lee E. ; Lee, Bok Y.: In vivo reflectance of blood and tissue as a function of light wavelength. In: *IEEE transactions on biomedical engineering* 37 (1990), Nr. 6, S. 632–639

[20] Mori, Hisao ; Yamamoto, Hareaki ; Kuwashima, Masaomi ; Saito, Saburo ; Ukai, Hiroshi ; Hirao, Kouichi ; Yamauchi, Mikio ; Umemura, Satoshi: How does deep breathing affect office blood pressure and pulse rate? In: *Hypertension research* 28 (2005), Nr. 6, S. 499–504

[21] Medical Instrumentation, Association for the Advancement o. u. a.: American national standard. Electronic or automated sphygmomanometers. In: *ANSI/AAMI SP10-1992/A1* (1996)

[22] O'Brien, Eoin ; Petrie, James ; Littler, WA ; Swiet, Michael de ; Padfield, Paul L. ; Altman, Douglas ; Bland, Martin ; Coats, Andrew ; Atkins, Neil u. a.: The British Hypertension Society protocol for the evaluation of blood pressure measuring devices. In: *J hypertens* 11 (1993), Nr. Suppl 2, S. S43–S62